frontiers in Materials

ORIGINAL RESEARCH
published: 25 January 2022
doi: 10.3389/fmats.2022.831725

Highly Efficient MoS_2/Cs_xWO_3 Nanocomposite Hydrogen Gas Sensors

Chang-Mou Wu, Shrisha, Kebena Gebeyehu Motora, Guan-Ying Chen, Dong-Hau Kuo and Noto Susanto Gultom*

Department of Materials Science and Engineering, National Taiwan University of Science and Technology, Taipei, Taiwan

Hydrogen gas sensors are important because of the significant use of hydrogen in industrial and commercial applications. In this study, we synthesized a novel Cs_xWO_3/MoS_2 nanocomposite using a solvothermal method. The samples were spin-coated on Si/SiO_2 substrates, and the sensors were fabricated with interdigital electrodes. The hydrogen gas sensing properties of the sensor were investigated. Cs_xWO_3/MoS_2 exhibited an outstanding hydrogen gas sensing ability at room temperature. In particular, the nanocomposite comprising 15 wt.% MoS_2 (15% Cs_xWO_3/MoS_2) showed a 51% response to hydrogen gas at room temperature. Further, it exhibited an excellent cyclic stability for hydrogen gas sensing, which is crucial for practical applications. Therefore, this study facilitates the development of effective and efficient hydrogen gas sensors operable at room temperature.

Keywords: Cs_xWO_3/MoS_2 nanocomposites, hydrogen gas, room temperature, sensors, metal oxide gas sensor

OPEN ACCESS

Edited by:
Mohammed M. Rahman, King Abdulaziz University, Saudi Arabia

Reviewed by:
Raid Ismail, University of Technology, Iraq, Iraq
Sanjit Manohar Majhi, United Arab Emirates University, United Arab Emirates
Franz Dickert, University of Vienna, Austria

****Correspondence:***
Chang-Mou Wu
cmwu@mail.ntust.edu.tw

Specialty section:
This article was submitted to Semiconducting Materials and Devices, a section of the journal Frontiers in Materials

Received: *08 December 2021*
Accepted: *06 January 2022*
Published: *25 January 2022*

Citation:
Wu C-M, Shrisha, Motora KG, Chen G-Y, Kuo D-H and Gultom NS (2022) Highly Efficient MoS_2/Cs_xWO_3 Nanocomposite Hydrogen Gas Sensors. Front. Mater. 9:831725. doi: 10.3389/fmats.2022.831725

INTRODUCTION

A polluted atmosphere endangers the health of living organisms. It comprises various gases that exist in nature and those released from industries (Masteghin et al., 2019; Pisarkiewicz et al., 2020; Duc et al., 2020; Kim et al., 2021). These odorless, tasteless, colorless gases are toxic when they exceed the safe limits (Ha et al., 2018; Miglietta et al., 2020; Pisarkiewicz et al., 2020). Hydrogen (H_2), carbon dioxide (CO_2), carbon monoxide (CO), and ammonia (NH_3) present in the environment have adverse effects on human health when their concentrations exceed the permissible levels (Annanouch et al., 2021; Hübert et al., 2014; Saravanan et al., 2017). Therefore, the amount of these gases in the environment must be monitored, and the development of effective and efficient detection methods is essential.

Hydrogen is one of the most hazardous gas and regulating its concentration with adequate monitoring devices is crucial (Hübert et al., 2014). Currently it is extensively used as a major ecological energy source and is used in semiconductor processing, chemical industry, nuclear reactors, and petroleum extraction. Hydrogen is a potential candidate for next-generation energy requirements in power plants, automobile transportation, and aerospace industries. However, the storage and regulated supply of hydrogen are challenging owing to the potential dangers of leakage (Saravanan et al., 2017). Therefore, developing long-lasting and cost-effective hydrogen sensing devices that are highly reliable for the accurate detection of the hazardous hydrogen gas is compelling (Hienuki et al., 2021; Liang et al., 2021; Sridhar et al., 2021).

In recent years, tungsten-based materials have gained a lot of interest owing to their nanostructures and unique chemical and physical properties (Chala et al., 2017; Motora and

Wu, 2020; Wu et al., 2019). Because of their good selectivity and stability, they are the most suitable for fabricating high-grade sensors. In particular, tungsten trioxide has been extensively used in sensors for the detection of hazardous gases, such as hydrogen, ammonia, nitrous oxide, and hydrogen sulfide (Wang et al., 2000; Rydosz et al., 2014; Castillo et al., 2020; Dong et al., 2020). However, most of the WO_3-based gas sensors function at high temperatures or have high response/recovery times, which hinder their practical application (Esfandiar et al., 2014; Chang et al., 2020). Therefore, the development of tungsten oxide-based gas sensor materials that can circumvent these limitations is important. In our previous study, we proposed a new tungsten bronze material-cesium tungsten oxide (Cs_xWO_3) for hydrogen gas sensors, which exhibited significant hydrogen gas sensing properties at room temperature owing to its mixed-valence state and unique properties (Wu et al., 2021). However, its sensor response and response time need to be enhanced to detect hydrogen gas within a short duration, which are crucial for practical applications. Therefore, to circumvent this limitation, a suitable sensor material should be selected.

In contrast, molybdenum disulfide is a transition metal dichalcogenide (TMD), which is used in various applications, such as photocatalysis, sensing, disinfection, contaminant adsorption, and membrane-based separation (Barua et al., 2017; Li et al., 2018; Bello et al., 2020). It has been applied in the field of sensors as photochemical sensors, gas sensors, glucose sensors, photodetectors, electrochemical sensors, and DNA sensors (Zhang et al., 2015; Akbari et al., 2018). Among the different types of gases, MoS_2 nanostructures are usually selective toward NH_3 gas at room temperature, which hinders their applicability as gas sensors. Although MoS_2 is a good sensing material, it has limitations, such as a low structural strength and conductivity (Huaning et al., 2021). However, few studies have shown that its selective behavior can change while forming hybrids with different materials; this can be ascribed to the charge-transfer-based modulation of the channel conductivity of the gas sensor mechanism (Gottam et al., 2020). Therefore, combining MoS_2 with unique material is important for achieving an enhanced sensing performance. For instance, WO_3/MoS_2 composites have been developed, and the nanocomposite exhibits excellent ammonia and hydrogen sulfide sensing properties (Singh et al., 2020, Singh et al., 2021). However, these sensor devices function only at temperatures higher than 200°C. Besides, most of the previously developed hydrogen gas sensor exhibited low sensor response. It is very important to develop hydrogen gas sensor with high sensitivity, selectivity, and stability for practical applications. Therefore, the development of MoS_2 composites with excellent hydrogen sensing performance at room temperature is crucial.

Herein, we developed Cs_xWO_3@MoS_2 nanocomposites for application in hydrogen gas sensors through a solvothermal method by taking advantage of the low-temperature sensing properties of Cs_xWO_3 and the high sensor response of MoS_2. The hydrogen gas sensing properties of the developed Cs_xWO_3@MoS_2 nanocomposite gas sensor at room temperature were systematically investigated. The proposed gas-sensing mechanism of the sensor was also explained.

MATERIALS AND METHODS

Materials

The tungsten hexachloride (WCl_6), cesium hydroxide ($CsOHH_2O$), anhydrous ethanol, and acetic acid were purchased from Kanto Chemical Co., Inc. Molybdenum disulfide powder (<2 μm, 98%) and N, N-dimethylformamide (DMF) were purchased from Sigma Aldrich.

All reagents and chemicals used in this study were of analytical grade and were used without further purification.

Synthesis of Cs_xWO_3 Nanorods

Tungsten hexachloride (0.2976 g) was added to anhydrous ethanol (40 ml) under intense stirring, resulting in the formation of a yellowish solution. Thereafter, 0.065 g of $CsOH{\cdot}H_2O$ was introduced into the yellowish solution. After the resultant solution became homogeneous, 10 ml of acetic acid was added. Subsequently, the mixture was transferred into a 100 ml Teflon-lined autoclave, followed by hydrothermal treatment at 240°C for 20 h. Afterward, it was cooled to room temperature naturally, and the blue product was centrifuged, washed with ethanol several times, and finally dried in a vacuum oven at 60°C for 8 h (Wu et al., 2021).

Exfoliation of MoS_2 Nanosheets

The MoS_2 nanosheets were exfoliated by ultrasonication according to a previously reported method (Bera and sciences, 2017). Bulk MoS_2 (0.64 g) was added to DMF (20 ml) in a flat-bottomed beaker (100 ml) and ultrasonicated for 60 min. The temperature of the sonication was controlled by a cooling system during ultrasonication. Afterward, the sample was centrifuged, washed, and dried at 60°C for 8 h.

Preparation of Cs_xWO_3/MoS_2 Nanocomposites

The Cs_xWO_3/MoS_2 nanocomposite was prepared using a hydrothermal method. The material required for the synthesis—0.1 M aqueous solution of MoS_2 (30 ml) was stirred for 1 h. Simultaneously, 0.2976 g of tungsten hexachloride was mixed with 40 ml of anhydrous ethanol under intense stirring, which resulted in the formation of a yellowish solution. Thereafter, 0.065 g of $CsOH{\cdot}H_2O$ was added to the yellowish solution. Subsequently, 10 ml of acetic acid was added to the resultant solution when it became homogeneous. Afterward, different amounts of the prepared MoS_2 solution were added to form composites with different ratios. Subsequently, the mixture was transferred into a 100 ml Teflon-lined autoclave, followed by a hydrothermal process at 240°C for 20 h. The obtained dark blue product was centrifuged, washed with ethanol several times, and finally

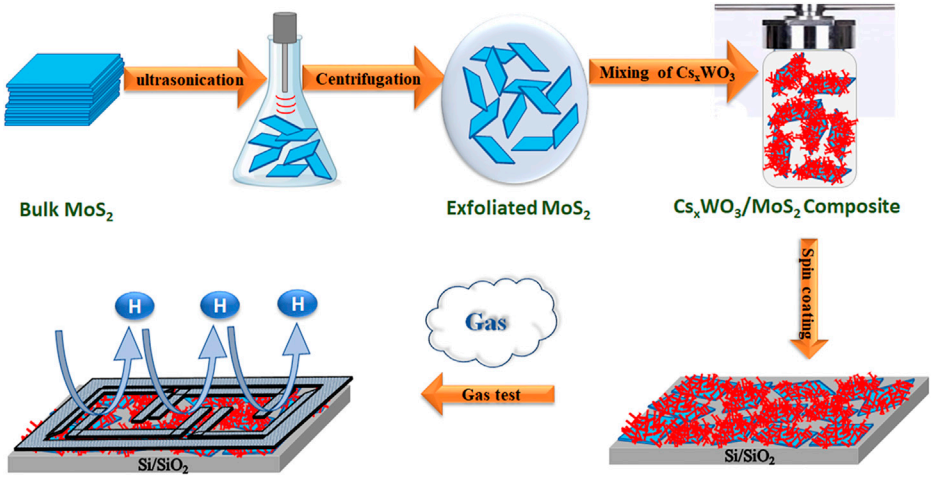

FIGURE 1 | Schematic illustration of the synthesis process of Cs_xWO_3/MoS_2-based gas sensor.

dried in a vacuum oven at 60°C. In this study, three different composites were prepared by changing the amount of MoS_2 and labeled as 5%, 15%, and 30%.

Characterization of Cs_xWO_3/MoS_2 Nanocomposites

Field emission scanning electron microscopy (FESEM, JSM6500F, JEOL, Tokyo, Japan), transmission electron microscopy (TEM), and high-resolution TEM (TEM, Philips-6500F) were used to study the surface morphologies of the samples. The crystal structures of the Cs_xWO_3, MoS_2, and Cs_xWO_3/MoS_2 nanocomposites were obtained by X-ray diffraction (XRD; D2 Phaser X-ray diffractometer, Bruker, Karlsruhe, Germany) analysis. The chemical compositions of the prepared samples were determined by Raman spectroscopy using an HR800 instrument (Jobin Yvon, Taipei, Taiwan). The N_2 adsorption/desorption isotherm and Brunauer, Emmett, and Teller (BET) surface area analyses of the samples were conducted at 77 K using a Quanta chrome iQ-MP gas adsorption analyzer (BEL JAPAN, INC.).

Sensor Fabrication and Hydrogen Gas Sensing Measurements

To fabricate the gas sensor, the as-prepared Cs_xWO_3, MoS_2, and Cs_xWO_3/MoS_2 nanocomposites were diluted with isopropanol (IPA) and spin-coated on Si/SiO_2 substrates, which were then sputtered with multi-finger Pt interdigitated electrodes (**Figure 1**). The H_2 gas sensing properties of the prepared sensors were measured in a compact vacuum chamber with an H_2 flow of 99.9% (diluted with dry air) *via* a mass flow controller. The properties were measured systematically from the electrical output response recorded using a Keithley source meter unit (SMU, Keithley 2,400, Tektronix, Beaverton, OR, USA) connected to a computer.

Electrochemical Measurements of the Sensors

The electrochemical properties of the developed sensor materials were investigated by electrochemical impedance spectroscopy (EIS) using a 5,000 electrochemical workstation (Jiehan Technology Corp., Taiwan), wherein a conventional three-electrode configuration was used. In this measurement, 0.1 M aqueous solution of KCl was used as the electrolyte and platinum and Ag/AgCl were used as the counter and reference electrodes, respectively; a titanium substrate was used as the working electrode (Phuruangrat et al., 2009). To prepare the working electrode for EIS measurements, 4 mg of Cs_xWO_3, MoS_2, and 15% Cs_xWO_3/MoS_2 were added to 80 µL of Nafion solution and 920 µL of absolute ethanol, and the mixture was ultrasonicated for approximately 90 min to obtain a slurry. Thereafter, 40 µL of the slurry was drop-cast onto a 1 × 1 cm^2 titanium substrate electrode and dried at room temperature.

RESULTS AND DISCUSSION

Morphological and Structural Properties of Cs_xWO_3/MoS_2 Nanocomposites

The surface morphologies of the prepared samples were studied by FESEM, and the FESEM image in **Figure 2A** shows that MoS_2 has a sheet-like morphology, mostly smaller than 2 µm in size. The FESEM image in **Figure 2B** depicts that the surface morphology of Cs_xWO_3 comprises a nanorod-like structure with an average diameter of 40–50 nm. The FESEM image of the 15% Cs_xWO_3/MoS_2 nanocomposite in **Figure 2C** shows the coexistence of nanorods and nanosheets, owing to surface morphologies of Cs_xWO_3 and MoS_2, confirming the successful synthesis of the intended nanocomposites. Furthermore, the corresponding EDS spectrum confirmed the existence of Mo and S from MoS_2; Cs, O, and W from Cs_xWO_3. The actual elemental composition of the 15% Cs_xWO_3/MoS_2 nanocomposite

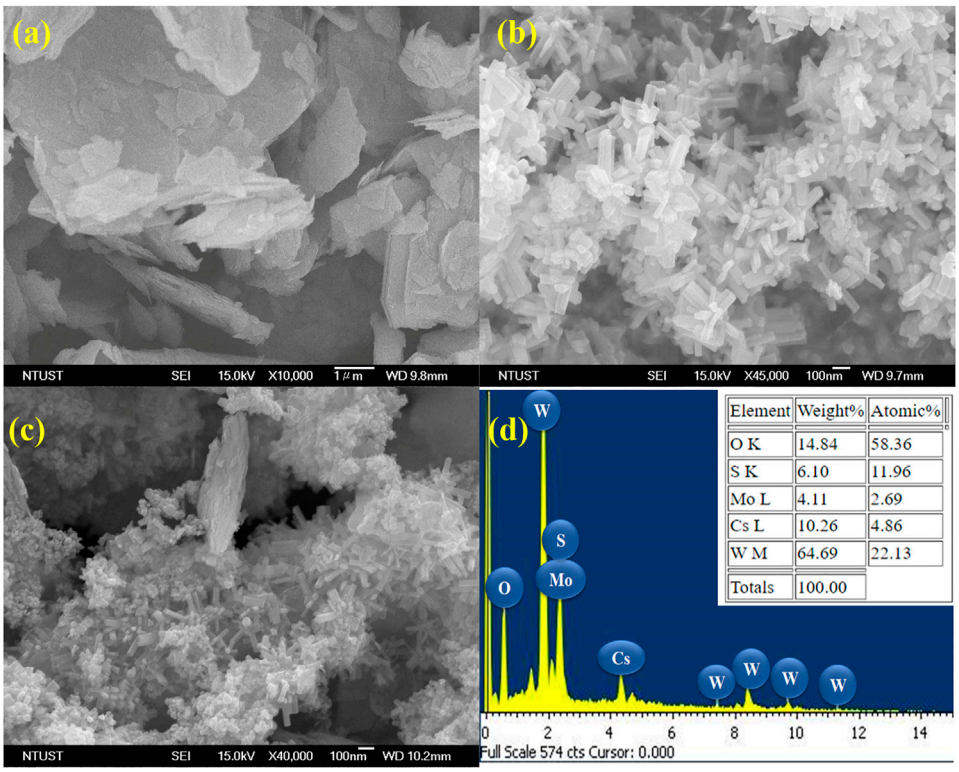

FIGURE 2 | FESEM images of **(A)** MoS_2 nanosheets; **(B)** Cs_xWO_3 nanorods; **(C)** Cs_xWO_3/MoS_2 composites and **(D)** EDS Spectrum of 15% Cs_xWO_3/MoS_2 nanocomposites.

was also investigated and the result as shown in the inset of **Figure 2D**. It can be seen from the actual mass percentage and theoretical mass percentage of each element in the nanocomposites that they are almost the same. These results reveal that the Cs_xWO_3/MoS_2 nanocomposite was successfully prepared.

The FESEM image in **Figure 3A** and elemental mapping results of the 15% Cs_xWO_3/MoS_2 nanocomposites presented in **Figures 3B–F** show the homogeneous distribution of Mo, S, Cs, O, and W elements in the nanocomposite.

The surface morphology of the synthesized 15% Cs_xWO_3/MoS_2 nanocomposite was further studied by TEM and HRTEM. The TEM image of 15% Cs_xWO_3/MoS_2 nanocomposite shown in **Figure 4A** can be ascribed to Cs_xWO_3 nanorods and MoS_2 nanosheets. The coexistence of the MoS_2 nanosheets and Cs_xWO_3 nanorods can be seen in the HRTEM image of the nanocomposite, as shown in **Figure 4B**. The lattice spacing of 0.32 nm corresponds to the (002) crystal plane of Cs_xWO_3 and that of 0.27 nm corresponds to the (100) crystal plane of MoS_2. The corresponding selected area electron diffraction (SAED) pattern in **Figure 4C** confirms the combination of both Cs_xWO_3 and MoS_2, where the dots forming the hexagonal shape are attributed to the MoS_2 nanosheets and those forming the triangle are ascribed to Cs_xWO_3 (Ahmadi et al., 2014). However, the SAED dots in **Figure 4C** form hexagonal and triangular shapes with minimal changes than those of individual Cs_xWO_3 and MoS_2. This can be attributed to the nanocomposite formation of Cs_xWO_3/MoS_2. These results confirm that the nanocomposite was successfully prepared, and the Cs_xWO_3 nanorods and MoS_2 nanosheets were in good contact, which would enhance the gas sensing property.

Figure 5 shows the XRD patterns of the $CxWO_3$ nanorods, MoS_2 nanosheets, and their nanocomposites. The XRD pattern of the Cs_xWO_3 nanorods can be ascribed to the hexagonal phase of $Cs_{0.33}WO_3$ (JCPDS No. 83-1334) (Wu et al., 2021). The absence of additional diffraction peaks confirmed the successful synthesis of pure $Cs_{0.33}WO_3$. The XRD peaks of the MoS_2 nanosheets can be indexed to hexagonal phase of MoS_2 (JCPDS No. 65-1951) (Zhang et al., 2014). The XRD peaks of the Cs_xWO_3/MoS_2 nanocomposites comprise characteristic peaks of both Cs_xWO_3 and MoS_2, confirming the successful preparation of the nanocomposite. In addition, the peak intensity of Cs_xWO_3 at (200) diffraction peak decreases as the MoS_2 content increases. The crystallite size of the Cs_xWO_3 and MoS_2 in the synthesized 15% Cs_xWO_3/MoS_2 nanocomposite was determined by using the Scherrer equation as shown below:

$$D = \frac{0.9\lambda}{\beta \cos\theta} \quad (1)$$

where λ is the wavelength of X-ray used (0.154 nm), β is the full-width at the half maximum of the respective diffraction peak, and θ is the angle at the maximum peak (Bekena et al., 2019). The

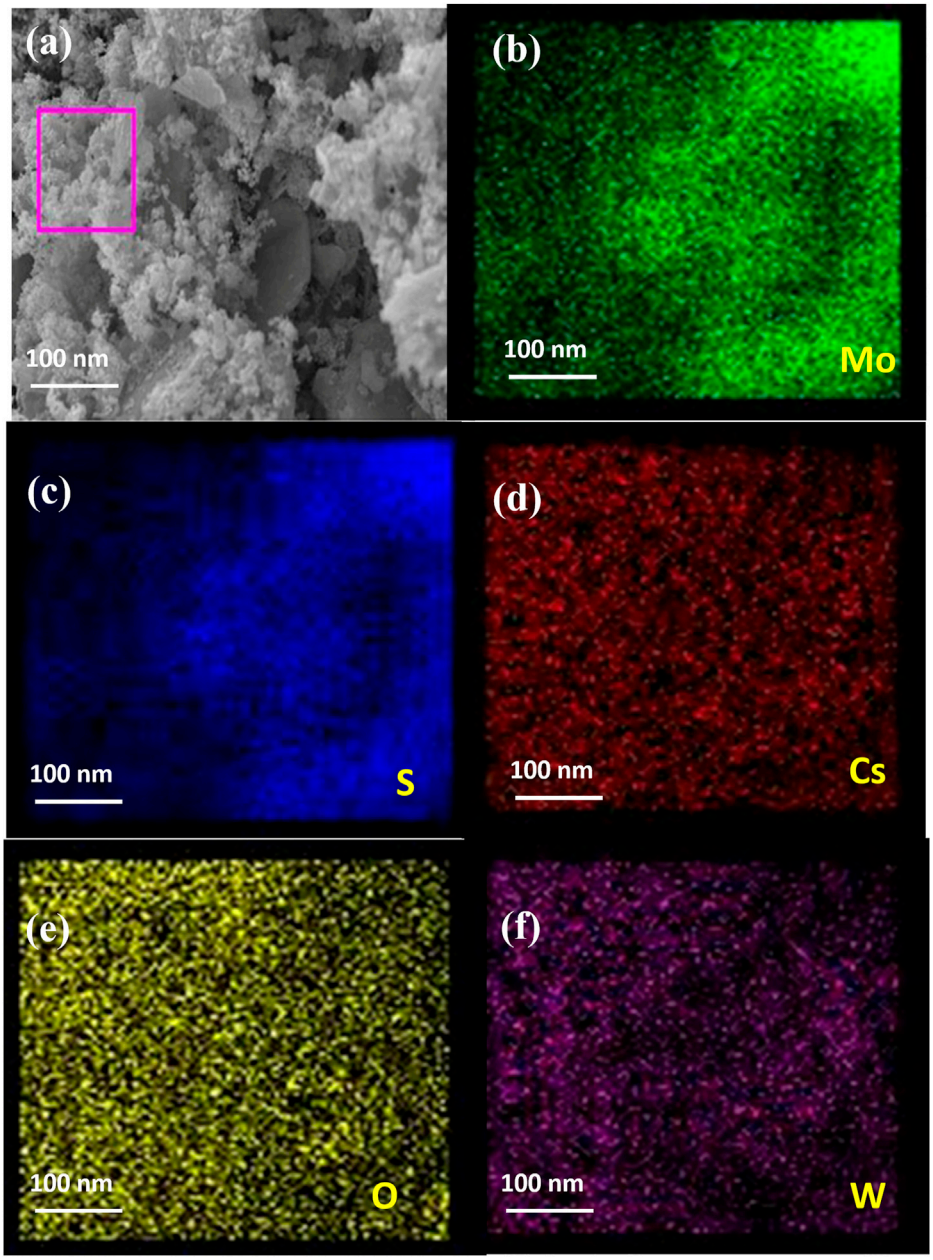

FIGURE 3 | (A) FESEM image and elemental mapping of **(B)** Mo, **(C)** S, **(D)** Cs, **(E)** O, and **(F)** W of 15% Cs_xWO_3/MoS_2 nanocomposite.

finding shows that the crystallite size of Cs_xWO_3 was 2 nm at diffraction peak of (200). While that of the MoS_2 nanocomposite is about 6 nm at (002) diffraction peak.

The as-prepared samples were further characterized by Raman spectroscopy, and the Raman spectra are shown in **Figure 6A**. The spectra show that two major peaks were observed for the MoS_2 nanosheets, which be indexed to the 2H phase of MoS_2 and E_{2g} (308 cm^{-1}) and A_{1g} (408 cm^{-1}) activation modes (Vadivelmurugan et al., 2021). The E_{2g} mode corresponds to the plane vibration of S and Mo atoms, whereas the A_{1g} mode is attributed to the relative vibration of the S atom, which is in the plane direction (Yao et al., 2019). Further, the two weak peaks at 451 and 1599 cm^{-1} indicate E_{1g} and the longitudinal acoustic phonon modes, respectively. In the case of Cs_xWO_3, the Raman peak at 731 cm^{-1} corresponds to monoclinic Gama WO_3 and that at 935 cm^{-1} corresponds to nanocrystalline Cs_xWO_3 (Okada et al., 2019). These peaks in Cs_xWO_3 confirm the nanocrystalline formation of WO_3 with cesium. The characteristic peaks of both MoS_2 and Cs_xWO_3 were observed for Cs_xWO_3/MoS_2 composite, indicating the successful preparation of the nanocomposites. In addition, there is a slight shift in the WO_3 peaks, at 872 and 993 cm^{-1}, which

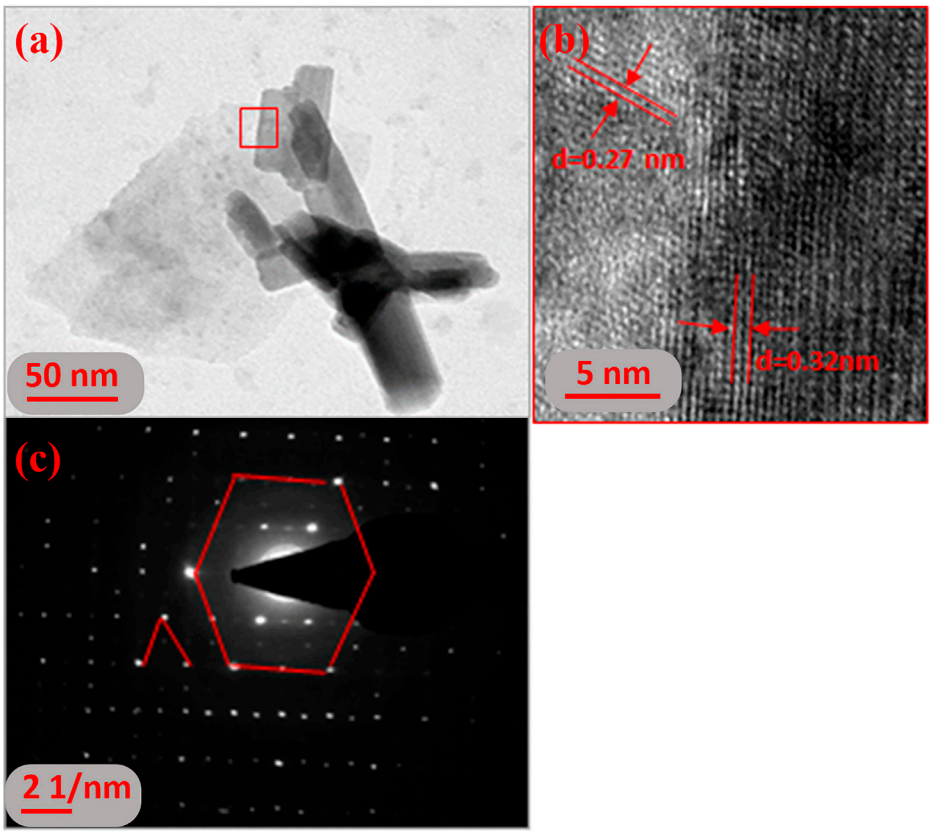

FIGURE 4 | (A) TEM, **(B)** HRTEM, and **(C)** SAED pattern images of 15% Cs_xWO_3/MoS_2 nanocomposite.

indicates the presence of different organizations of elemental WO_6 octahedral.

The BET specific surface areas of the materials were investigated by N_2 adsorption analysis, and the results in **Figure 6B** show that all the samples exhibited N_2 adsorption-desorption isotherms similar to type IV curves according to the Brunauer-Deming-Deming-Teller classification (Wang et al., 2018). The specific surface areas of the pure Cs_xWO_3, pure MoS_2, and 15% Cs_xWO_3/MoS_2 nanocomposites were calculated from the linear region of the multipoint plot. The BET specific surface areas of Cs_xWO_3, MoS_2, and 15% Cs_xWO_3/MoS_2 nanocomposites were 31.1, 3.3, and 15.0 m^2g^{-1}, respectively. Herein, the surface area of 15% Cs_xWO_3/MoS_2 was lower than that of pure Cs_xWO_3 because of the encompassing of the nanorods by the MoS_2 nanosheets. Compared to MoS_2 nanosheets, the 15% Cs_xWO_3/MoS_2 nanocomposites possessed a larger surface area, which is important for the adsorption of a higher amount of hydrogen gas, and would aid in enhancing the gas sensing properties of the sensor.

Hydrogen Gas Sensing Properties of Cs_xWO_3/MoS_2 Composites-Based Gas Sensors

The sensing properties of metal oxide-based gas sensors are usually measured in terms of their sensitivity and repeatability by varying the resistance values of gas and vacuum/air *vs.* time. The H_2 gas detection properties of the Cs_xWO_3/MoS_2 nanocomposites were tested at a gas concentration of 10–500 ppm at 25°C (~ 35 RH %). The sensor response of the samples is calculated using **Equation 2** for oxidizing gases and vice versa for reducing gases.

$$S(\%) = \frac{R_g}{R_a} \times 100 \quad (2)$$

where R is the resistance; a is the air atmosphere, and g is the gas atmosphere of the samples.

The gas-sensing performance of a sensor can be determined using the current-voltage (I-V) curve recorded before and after the adsorption of the gas. Herein, we also evaluated the H_2 gas sensing performance of 15% Cs_xWO_3/MoS_2 nanocomposites using I-V characteristics before and after the adsorption of hydrogen gas, and the results in **Figure 7A** show the change in the electrical performance in the presence of H_2 when compared with that of no hydrogen gas. **Figure 7B** shows the sensor response of the developed 15% Cs_xWO_3/MoS_2 nanocomposite gas sensor at different concentrations (500, 250, 100, and 10 ppm) of hydrogen gas. The developed sensor exhibited outstanding H_2 gas sensing properties with a 50.6% sensor response toward 500 ppm of H_2 gas with 60 and 120 s response and recovery time, respectively. These recovery time and

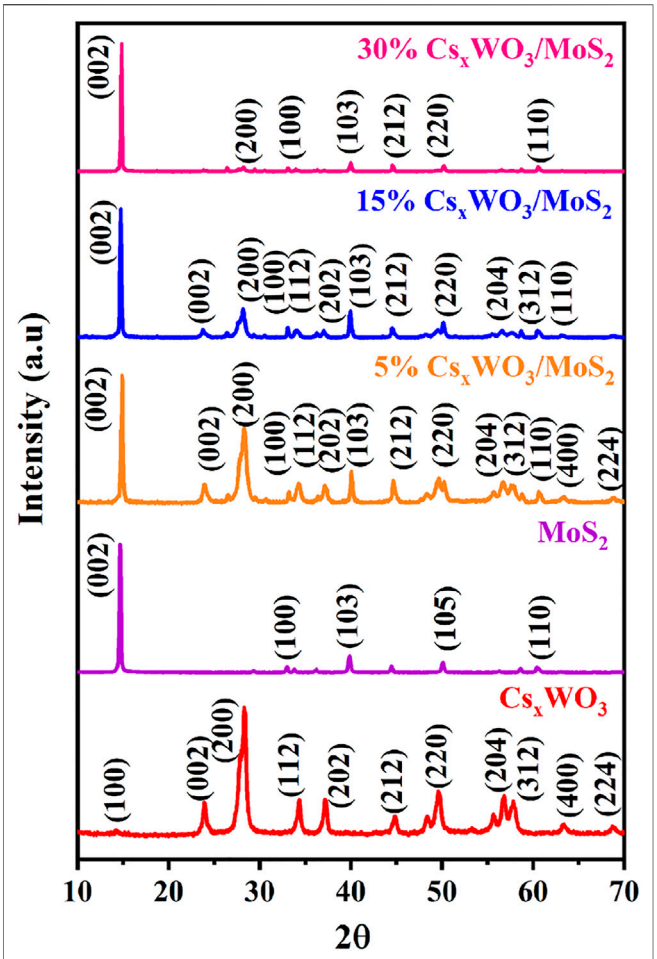

FIGURE 5 | XRD results of pure Cs_xWO_3, pure MoS_2, and different ratios of Cs_xWO_3/MoS_2 nanocomposites.

response time are better than that of reported Pd/CNT/Ni H_2 gas sensor that has 312 s response time and 173 s recovery and Ni/Pd-graphene H_2 gas, which has 180 s response time and 720 s recover time. (Lin and Huang, 2012; Phan and Chung, 2014). This sensor response is superior to that of the H_2 gas sensor of pure Cs_xWO_3 (31.3%) (Wu et al., 2021), which indicates that nanocomposite formation has enhanced the sensitivity. **Figure 7C** presents the sensor response *vs*. concentration curve, which shows a linear increase in the sensor response with an increase in concentration, revealing that the developed sensor can be applied to detect a wide range of concentrations of H_2 gas. **Figure 7D** shows that the fabricated 15% Cs_xWO_3/MoS_2 nanocomposite H_2 gas sensor demonstrates excellent cyclic stability for the five consecutive cycles that are important for practical applications. These findings reveal the potential applicability of the developed 15% Cs_xWO_3/MoS_2 nanocomposite sensor for the detection of H_2 gas.

Long-term stability of sensor is very important for practical application. Herein, the long-term stability of the developed sensor was investigated. The result as shown in **Figure 8A** shows that it has excellent long-term stability during the 11-days evaluation period. Moreover, selectivity of the fabricated 15% Cs_xWO_3/MoS_2 nanocomposite hydrogen gas sensor was also studied. The finding in **Figure 8B** indicates that the 15% Cs_xWO_3/MoS_2 nanocomposite sensor presented excellent selectivity towards hydrogen gas by showing only 4 and 5% sensor response toward ammonia and carbon dioxide, respectively. The sensor response of the developed sensor toward CO_2 and NH_3 is neglible when compared with that of H_2 (50.6%). These findings confirm that developed sensor has potential applicability for real application for H_2 gas sensing. The sensing property of the developed sensor with respect to current versus time was also investigated. As it can be seen in **Supplementary Figure S1**, the current response of the fabricated sensor increases with increasing H_2 gas concentration, which proves the behavior of the n-type semiconductor sensor (Wisitsoraat et al., 2009; Mohamad et al., 2010). Moreover, the pure Cs_xWO_3 and MoS_2 also have the same properties (Saravanan et al., 2019; Wu et al., 2021).

Figure 9 shows the sensor response of Cs_xWO_3/MoS_2 nanocomposites against different amount of MoS_2 (5%, 15%, and 30%) added to Cs_xWO_3. The sensor response of the nanocomposite initially increased with an increase in the amount of MoS_2 up to 15% MoS_2 addition and then decreased

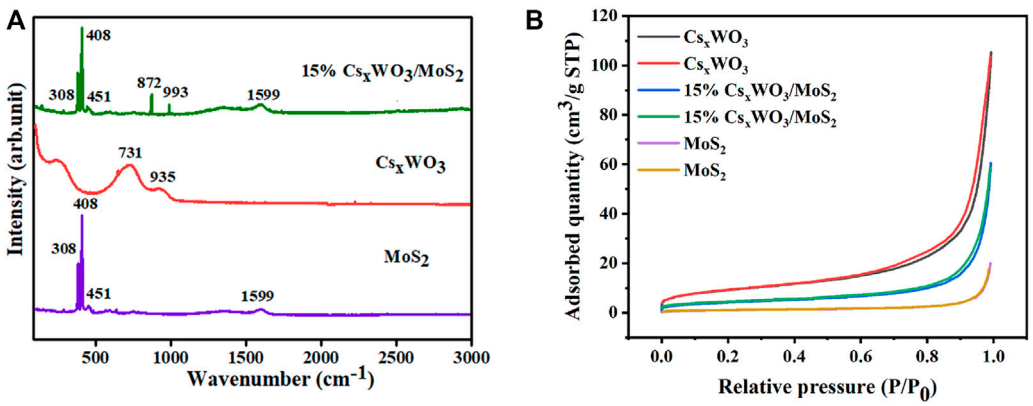

FIGURE 6 | (A) Raman spectra and **(B)** N_2 adsorption-desorption isotherms of the pure Cs_xWO_3, pure MoS_2, and 15% Cs_xWO_3/MoS_2 nanocomposite.

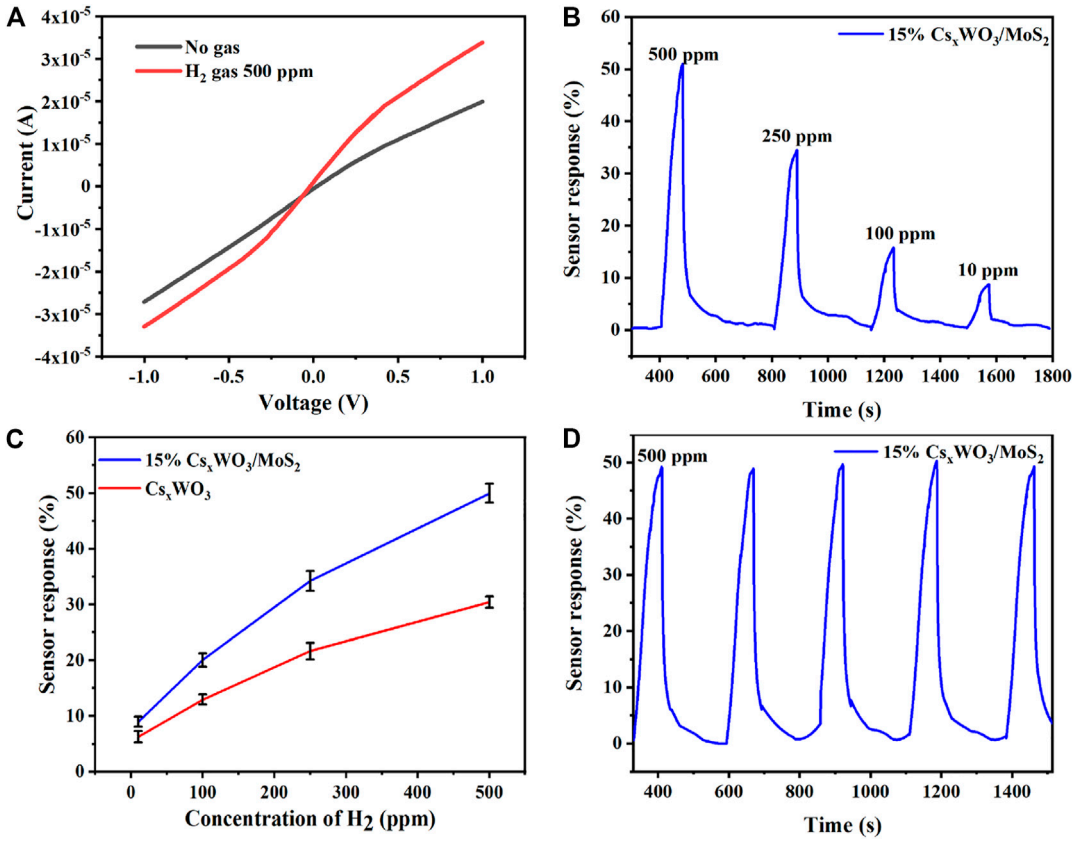

FIGURE 7 | (A) I-V curves, **(B)** sensor response with respect to the H_2 gas concentration of 15% Cs_xWO_3/MoS_2-based hydrogen gas sensor, **(C)** variation of the sensing response of Cs_xWO_3 and 15% Cs_xWO_3/MoS_2-based hydrogen gas sensor at room temperature when exposed to different ppm hydrogen, and **(D)** repeatability of 15% Cs_xWO_3/MoS_2-based hydrogen gas sensor at 500 ppm.

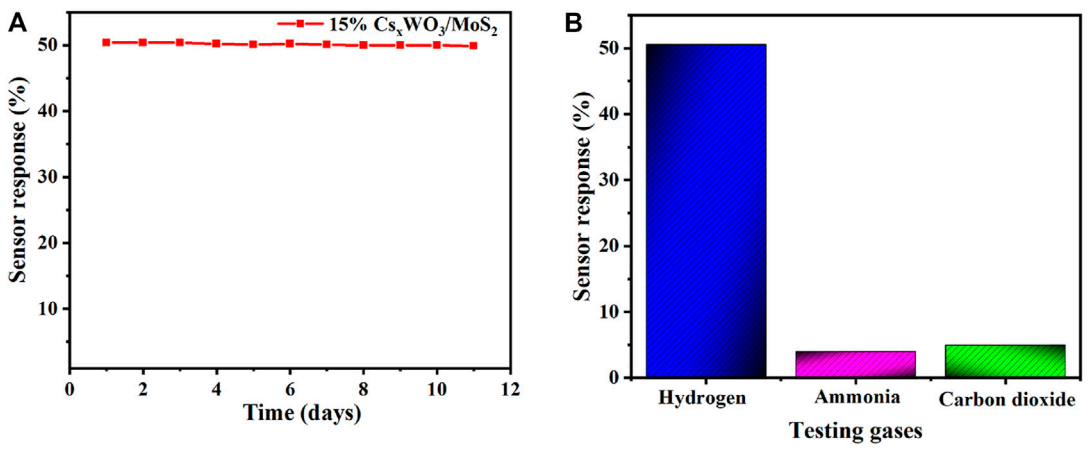

FIGURE 8 | (A) long-term stability, and **(B)** selectivity of the 15% Cs_xWO_3/MoS_2-based hydrogen gas sensor.

till 30% MoS_2 addition. This could be because of the encompassing of $CsxWO_3$ nanorods by MoS_2 nanosheets with low surface areas, which influences the adsorption of H_2 gas and consequently the sensor response (**Supplementary Figure S2**). The photograph of the prepared samples dispersed in IPA shown in **Supplementary Figure S3** also confirms that the intensity of the dark color of the nanocomposite increases with an increase in the concentration of MoS_2 nanosheets, which confirms the

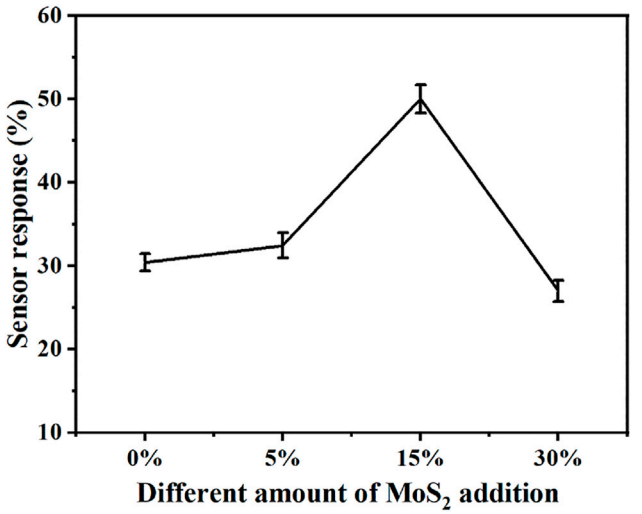

FIGURE 9 | Sensor response of the Cs_xWO_3/MoS_2 nanocomposite sensor with respect to amounts of MoS_2 added to Cs_xWO_3.

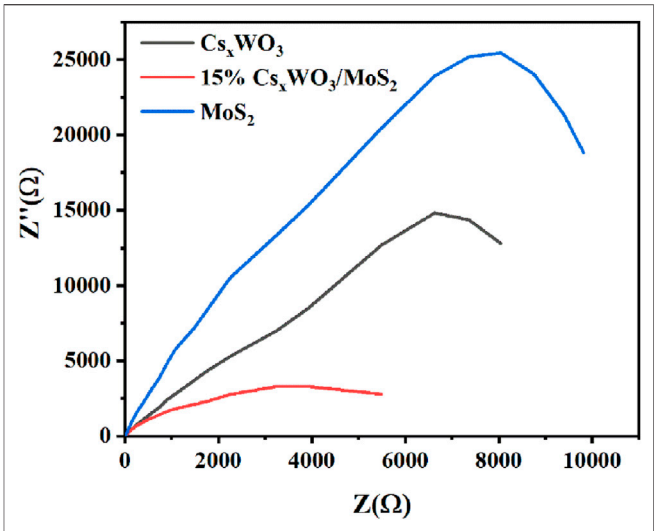

FIGURE 11 | Electrochemical impedance spectra of Cs_xWO_3, MoS_2, and 15% Cs_xWO_3/MoS_2.

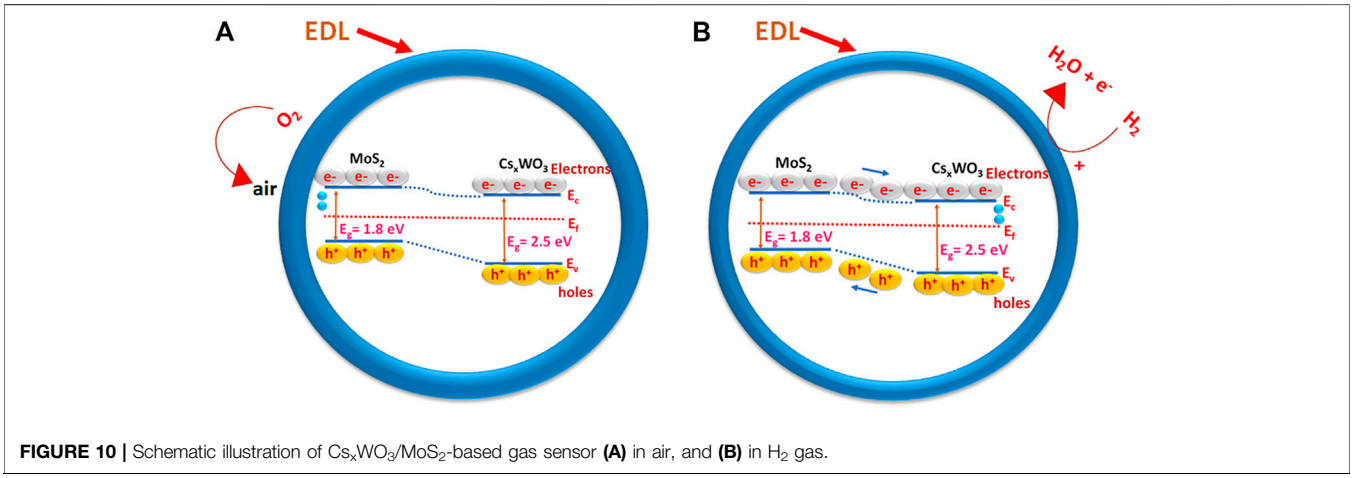

FIGURE 10 | Schematic illustration of Cs_xWO_3/MoS_2-based gas sensor **(A)** in air, and **(B)** in H_2 gas.

presence of the high amount of MoS_2 in 30% MoS_2. Therefore, 15% Cs_xWO_3/MoS_2 nanocomposite was selected for further studies.

Possible Hydrogen Gas Sensing Mechanisms of Cs_xWO_3/MoS_2 Nanocomposites

Metal oxide-based gas sensors, which sense hydrogen gas, are usually explained based on the variation of the electron depletion layer (EDL) and oxygen adsorption (Sun et al., 2011; Park et al., 2015; Wang et al., 2018). Herein, we propose a sensing mechanism for the developed sensor based on EDL. Cs_xWO_3 has oxygen defects in its structure, and MoS_2 is tuned to have a high bandgap after the exfoliation of bulk MoS_2. Therefore, the Cs_xWO_3 nanorods in the nanocomposite can adsorb oxygen from the air because of its oxygen vacancies, and the adsorbed oxygen extracts electrons from the conduction band and generates oxygen species and increases the width of the EDL (**Figure 10A**). In contrast, when the sensor is exposed to H_2 gas, the adsorbed oxygen species react with H_2 gas and produce extra electrons in the conduction band of $CsxWO_3$, which increase the electrical performance of the material and consequently the sensing property (**Figure 10B**).

Further, the electrochemical properties of the samples were investigated, and the results in **Figure 11** show that the EIS semicircle radius of the 15% Cs_xWO_3/MoS_2 nanocomposite is lower than those of pure Cs_xWO_3 and pure MoS_2, confirming that the nanocomposite has a higher electrical conductivity than those of pure materials, which contributed to the enhancement in the hydrogen gas sensor response.

The hydrogen gas sensing response of the developed 15% Cs_xWO_3/MoS_2 nanocomposite was also compared with those of reported hydrogen gas sensors, and the results in **Table 1** indicate

TABLE 1 | Comparison of H_2 sensing properties of different metal oxide-based gas sensors.

Materials	Sensing response (%)	Operating temp. (°C)	H_2 conc. (ppm)	References
MoS_2–Si	15.4	RT	5,000	Liu et al. (2015)
MoS_2 nanosheets	20.5	120	500	Zhang et al. (2018)
rGO–TiO_2	22	180	500	Esfandiar et al. (2012)
Graphene-Ag-Pd	9	RT	500	Sharma and Kim, (2018)
ZnO–graphene	3.5	150	500	Anand et al. (2014)
ZnO-Nanorods-In_2O_3	15	RT	500	Huang and Lin, (2012)
Cd-doped ZnO nanorods	1.6	80°C	500	Yang et al. (2015)
ZnO nanorods/In	20.5	RT	500	Huang and Lin, (2012)
WO_3 nanoparticles	7.5	350	5,000	Xiao et al. (2018)
Cs_xWO_3 nanorods	31.3	RT	500	Wu et al. (2021)
Pd/WO_3 films	27.5	25	5,000	Xiao et al. (2018)
Cs_xWO_3/MoS_2	50.6	RT	500	This work

that the 15% Cs_xWO_3/MoS_2 nanocomposite exhibited a higher sensor response than those of other sensors (Esfandiar et al., 2012; Huang and Lin, 2012; Anand et al., 2014; Liu et al., 2015; Yang et al., 2015; Zhang et al., 2018; Sharma and Kim, 2018; Xiao et al., 2018; Wu et al., 2021). Further, some of the reported sensors can only operate at high temperatures. Therefore, the developed 15% Cs_xWO_3/MoS_2 nanocomposite H_2 gas sensor is a promising candidate for practical application in the detection of hydrogen gas.

CONCLUSION

In this study, Cs_xWO_3/MoS_2 nanocomposites were successfully prepared using the solvothermal method. The developed Cs_xWO_3/MoS_2 nanocomposite-based sensor exhibited outstanding hydrogen gas sensing properties with 51% response to 500 ppm H_2 gas. It also exhibits excellent cyclic stability. Further, the developed 15% Cs_xWO_3/MoS_2 nanocomposite demonstrated a superior H_2 gas sensing response at room temperature compared to reported H_2 gas sensors. The enhanced sensing response could be because of the improved electrical properties of the 15% Cs_xWO_3/MoS_2 nanocomposite. Therefore, this study facilitates the development of an effective and efficient H_2 gas sensor at room temperature, which will play a crucial role in the detection of hydrogen gas in the environment.

DATA AVAILABILITY STATEMENT

The original contributions presented in the study are included in the article/**Supplementary Material**, further inquiries can be directed to the corresponding author.

AUTHOR CONTRIBUTIONS

C-MW: Supervision, conceptualization and reviewing and editing. Shrisha: Methodology, data curation and writing. KM: Review and editing. G-YC: Methodology and data curation. D-HK: Resources. NG: Methodology.

ACKNOWLEDGMENTS

We would like to acknowledge the Ministry of Science and Technology of Taiwan, ROC for financially supporting part of this work, under contract numbers: MOST 110-2622-E-011-023.

SUPPLEMENTARY MATERIAL

The Supplementary Material for this article can be found online at: https://www.frontiersin.org/articles/10.3389/fmats.2022.831725/full#supplementary-material

REFERENCES

Ahmadi, M., Younesi, R., and Guinel, M. J.-F. (2014). Synthesis of Tungsten Oxide Nanoparticles Using a Hydrothermal Method at Ambient Pressure. *J. Mater. Res.* 29, 1424–1430. doi:10.1557/jmr.2014.155

Akbari, E., Jahanbin, K., Afroozeh, A., Yupapin, P., and Buntat, Z. (2018). Brief Review of Monolayer Molybdenum Disulfide Application in Gas Sensor. *Physica B: Condensed Matter* 545, 510–518. doi:10.1016/j.physb.2018.06.033

Anand, K., Singh, O., Singh, M. P., Kaur, J., and Singh, R. C. (2014). Hydrogen Sensor Based on graphene/ZnO Nanocomposite. *Sensors Actuators B: Chem.* 195, 409–415. doi:10.1016/j.snb.2014.01.029

Annanouch, F. E., Martini, V., Fiorido, T., Lawson, B., Aguir, K., and Bendahan, M. (2021). Embedded Transdermal Alcohol Detection via a Finger Using SnO2 Gas Sensors. *Sensors* 21, 6852. doi:10.3390/s21206852

Barua, S., Dutta, H. S., Gogoi, S., Devi, R., and Khan, R. (2017). Nanostructured MoS2-Based Advanced Biosensors: A Review. *ACS Appl. Nano Mater.* 1, 2–25. doi:10.1021/acsanm.7b00157

Bekena, F. T., Abdullah, H., Kuo, D.-H., and Zeleke, M. A. (2019). Photocatalytic Reduction of 4-nitrophenol Using Effective Hole Scavenger over Novel Mg-Doped Zn(O,S) Nanoparticles. *J. Ind. Eng. Chem.* 78, 116–124. doi:10.1016/j.jiec.2019.06.029

Bello, I. T., Oladipo, A. O., Adedokun, O., and Dhlamini, S. M. (2020). Recent Advances on the Preparation and Electrochemical Analysis of MoS2-Based Materials for Supercapacitor Applications: A Mini-Review. *Mater. Today Commun.* 25, 101664. doi:10.1016/j.mtcomm.2020.101664

Castillo, C., Cabello, G., Chornik, B., Huentupil, Y., and Buono-Core, G. E. (2020). Characterization of Photochemically Grown Pd Loaded WO3 Thin Films and its Evaluation as Ammonia Gas Sensor. *J. Alloys Compd.* 825, 154166. doi:10.1016/j.jallcom.2020.154166

Chala, T., Wu, C.-M., Chou, M.-H., Gebeyehu, M., and Cheng, K.-B. (2017). Highly Efficient Near Infrared Photothermal Conversion Properties of Reduced Tungsten Oxide/polyurethane Nanocomposites. *Nanomaterials* 7, 191. doi:10.3390/nano7070191

Chang, C.-H., Chou, T.-C., Chen, W.-C., Niu, J.-S., Lin, K.-W., Cheng, S.-Y., et al. (2020). Study of a WO3 Thin Film Based Hydrogen Gas Sensor Decorated with Platinum Nanoparticles. *Sensors Actuators B: Chem.* 317, 128145. doi:10.1016/j.snb.2020.128145

Dong, C., Zhao, R., Yao, L., Ran, Y., Zhang, X., and Wang, Y. (2020). A Review on WO3 Based Gas Sensors: Morphology Control and Enhanced Sensing Properties. *J. Alloys Compd.* 820, 153194. doi:10.1016/j.jallcom.2019.153194

Duc, C., Boukhenane, M.-L., Wojkiewicz, J.-L., and Redon, N. (2020). Hydrogen Sulfide Detection by Sensors Based on Conductive Polymers: a Review. *Front. Mater.* 7, 215. doi:10.3389/fmats.2020.00215

Esfandiar, A., Ghasemi, S., Irajizad, A., Akhavan, O., and Gholami, M. R. (2012). The Decoration of TiO2/reduced Graphene Oxide by Pd and Pt Nanoparticles for Hydrogen Gas Sensing. *Int. J. Hydrogen Energ.* 37, 15423–15432. doi:10.1016/j.ijhydene.2012.08.011

Esfandiar, A., Irajizad, A., Akhavan, O., Ghasemi, S., and Gholami, M. R. (2014). Pd-WO3/reduced Graphene Oxide Hierarchical Nanostructures as Efficient Hydrogen Gas Sensors. *Int. J. Hydrogen Energ.* 39, 8169–8179. doi:10.1016/j.ijhydene.2014.03.117

Gottam, S. R., Tsai, C.-T., Wang, L.-W., Wang, C.-T., Lin, C.-C., and Chu, S.-Y. (2020). Highly Sensitive Hydrogen Gas Sensor Based on a MoS2-Pt Nanoparticle Composite. *Appl. Surf. Sci.* 506, 144981. doi:10.1016/j.apsusc.2019.144981

Ha, N. H., Thinh, D. D., Huong, N. T., Phuong, N. H., Thach, P. D., and Hong, H. S. (2018). Fast Response of Carbon Monoxide Gas Sensors Using a Highly Porous Network of ZnO Nanoparticles Decorated on 3D Reduced Graphene Oxide. *Appl. Surf. Sci.* 434, 1048–1054. doi:10.1016/j.apsusc.2017.11.047

Hienuki, S., Mitoma, H., Ogata, M., Uchida, I., and Kagawa, S. (2021). Environmental and Energy Life Cycle Analyses of Passenger Vehicle Systems Using Fossil Fuel-Derived Hydrogen. *Int. J. Hydrogen Energ.* 46, 36569–36580. doi:10.1016/j.ijhydene.2021.08.135

Huang, B.-R., and Lin, J.-C. (2012). Core-shell Structure of Zinc Oxide/indium Oxide Nanorod Based Hydrogen Sensors. *Sensors Actuators B: Chem.* 174, 389–393. doi:10.1016/j.snb.2012.08.065

Huaning, J., Huaizhang, W., and Ting, L. (2021). Research Progress of MoS2 Composite rGO Material in Gas Sensor. *E3S Web Conferences: EDP Sci.* 267, 02048. doi:10.1051/e3sconf/202126702048

Hübert, T., Boon-Brett, L., Palmisano, V., and Bader, M. A. (2014). Developments in Gas Sensor Technology for Hydrogen Safety. *Int. J. Hydrogen Energ.* 39, 20474–20483. doi:10.1016/j.ijhydene.2014.05.042

Kim, T., Lee, S., Cho, W., Kwon, Y. M., Baik, J. M., and Shin, H. (2021). Development of a Novel Gas-Sensing Platform Based on a Network of Metal Oxide Nanowire Junctions Formed on a Suspended Carbon Nanomesh Backbone. *Sensors* 21, 4525. doi:10.3390/s21134525

Li, Z., Meng, X., and Zhang, Z. (2018). Recent Development on MoS2-Based Photocatalysis: A Review. *J. Photochem. Photobiol. C: Photochem. Rev.* 35, 39–55. doi:10.1016/j.jphotochemrev.2017.12.002

Liang, L., Yang, Q., Zhao, S., Wang, L., and Liang, F. (2021). Excellent Catalytic Effect of LaNi5 on Hydrogen Storage Properties for Aluminium Hydride at Mild Temperature. *Int. J. Hydrogen Energ.* 46, 38733–38740. doi:10.1016/j.ijhydene.2021.09.130

Lin, T.-C., and Huang, B.-R. (2012). Palladium Nanoparticles Modified Carbon Nanotube/nickel Composite Rods (Pd/CNT/Ni) for Hydrogen Sensing. *Sensors Actuators B: Chem.* 162, 108–113. doi:10.1016/j.snb.2011.12.044

Liu, Y., Hao, L., Gao, W., Wu, Z., Lin, Y., Li, G., et al. (2015). Hydrogen Gas Sensing Properties of MoS2/Si Heterojunction. *Sensors Actuators B: Chem.* 211, 537–543. doi:10.1016/j.snb.2015.01.129

Masteghin, M. G., Godoi, D. R. M., and Orlandi, M. O. (2019). Heating Method Effect on SnO Micro-disks as NO2 Gas Sensor. *Front. Mater.* 6, 171. doi:10.3389/fmats.2019.00171

Miglietta, M., Alfano, B., Santos, J., Sayago, I., Polichetti, T., Massera, E., et al. (2020). "Outstanding NO_2 Sensing Performance of Sensors Based on TiO_2/Graphene Hybrid," in Proceeding of the AISEM Annual Conference on Sensors and Microsystems, February 2020 (Springer), 349–355.

Mohamad, M., Mustafa, F., Abidin, M. S. Z., Abd Rahman, S. F., Al-Obaidi, N. K. A., Hashim, A. M., et al. (2010). "The Sensing Performance of Hydrogen Gas Sensor Utilizing Undoped-AlGaN/GaN HEMT," in Proceeding of the 2010 IEEE International Conference on Semiconductor Electronics (ICSE2010), Malacca, Malaysia, June 2010 (IEEE). doi:10.1109/smelec.2010.5549369

Motora, K. G., and Wu, C.-M. (2020). Magnetically Separable Highly Efficient Full-Spectrum Light-Driven WO2.72/Fe3O4 Nanocomposites for Photocatalytic Reduction of Carcinogenic Chromium (VI) and Organic Dye Degradation. *J. Taiwan Inst. Chem. Eng.* 117, 123–132. doi:10.1016/j.jtice.2020.12.006

Okada, M., Ono, K., Yoshio, S., Fukuyama, H., and Adachi, K. (2019). Oxygen Vacancies and Pseudo Jahn-Teller Destabilization in Cesium-Doped Hexagonal Tungsten Bronzes. *J. Am. Ceram. Soc.* 102, 5386–5400. doi:10.1111/jace.16414

Park, S., Kim, S., Kheel, H., Park, S. E., and Lee, C. (2015). Synthesis and Hydrogen Gas Sensing Properties of TiO2-Decorated CuO Nanorods. *Bull. Korean Chem. Soc.* 36, 2458–2463. doi:10.1002/bkcs.10473

Phan, D.-T., and Chung, G.-S. (2014). Reliability of Hydrogen Sensing Based on Bimetallic Ni-Pd/graphene Composites. *Int. J. Hydrogen Energ.* 39, 20294–20304. doi:10.1016/j.ijhydene.2014.10.006

Phuruangrat, A., Ham, D. J., Thongtem, S., and Lee, J. S. (2009). Electrochemical Hydrogen Evolution over MoO3 Nanowires Produced by Microwave-Assisted Hydrothermal Reaction. *Electrochemistry Commun.* 11, 1740–1743. doi:10.1016/j.elecom.2009.07.005

Pisarkiewicz, T., Maziarz, W., Małolepszy, A., Stobiński, L., Michoń, D., and Rydosz, A. (2020). Multilayer Structure of Reduced Graphene Oxide and Copper Oxide as a Gas Sensor. *Coatings* 10, 1015. doi:10.3390/coatings10111015

Rydosz, A., Maziarz, W., Pisarkiewicz, T., Wincza, K., and Gruszczynski, S. (2014). "Deposition of Nanocrystalline Wo_3 and CuO Thin Film in View of Gas Sensor Applications," in Proceedings the Second International Conference on Technological Advances in Electrical, Electronics and Computer Engineering, Kuala Lumpur, Malaysia, March 2014.

Saravanan, A., Huang, B.-R., Kathiravan, D., and Prasannan, A. (2017). Natural Biowaste-Cocoon-Derived Granular Activated Carbon-Coated ZnO Nanorods: A Simple Route to Synthesizing a Core-Shell Structure and its Highly Enhanced UV and Hydrogen Sensing Properties. *ACS Appl. Mater. Inter.* 9, 39771–39780. doi:10.1021/acsami.7b11051

Saravanan, A., Huang, B.-R., Chu, J. P., Prasannan, A., and Tsai, H.-C. (2019). Interface Engineering of Ultrananocrystalline diamond/MoS2-ZnO Heterostructures and its Highly Enhanced Hydrogen Gas Sensing Properties. *Sensors Actuators B: Chem.* 292, 70–79. doi:10.1016/j.snb.2019.04.108

Sharma, B., and Kim, J.-S. (2018). Graphene Decorated Pd-Ag Nanoparticles for H2 Sensing. *Int. J. Hydrogen Energ.* 43, 11397–11402. doi:10.1016/j.ijhydene.2018.03.026

Singh, S., Deb, J., Sarkar, U., and Sharma, S. (2021). MoS2/WO3 Nanosheets for Detection of Ammonia. *ACS Appl. Nano Mater.* 4, 2594–2605. doi:10.1021/acsanm.0c03239

Singh, S., Dogra, N., and Sharma, S. (2020). A Sensitive H2S Sensor Using MoS2/WO3 Composite. *Mater. Today Proc.* 28, 8–10. doi:10.1016/j.matpr.2019.12.104

Sridhar, A., Ponnuchamy, M., Kumar, P. S., Kapoor, A., and Xiao, L. (2021). Progress in the Production of Hydrogen Energy from Food Waste: A Bibliometric Analysis. *Int. J. Hydrogen Energ.* doi:10.1016/j.ijhydene.2021.09.258

Sun, P., Sun, Y., Ma, J., You, L., Lu, G., Fu, W., et al. (2011). Synthesis of Novel SnO2/ZnSnO3 Core-Shell Microspheres and Their Gas Sensing Properities. *Sensors Actuators B: Chem.* 155, 606–611. doi:10.1016/j.snb.2011.01.017

Vadivelmurugan, A., Anbazhagan, R., Lai, J.-Y., and Tsai, H.-C. (2021). Paramagnetic Properties of Manganese Chelated on Glutathione-Exfoliated MoS2. *Colloids Surf. A: Physicochemical Eng. Aspects* 608, 125432. doi:10.1016/j.colsurfa.2020.125432

Wang, Z., Huang, S., Men, G., Han, D., and Gu, F. (2018). Sensitization of Pd Loading for Remarkably Enhanced Hydrogen Sensing Performance of 3DOM WO3. *Sensors Actuators B: Chem.* 262, 577–587. doi:10.1016/j.snb.2018.02.041

Wang, X., Miura, N., and Yamazoe, N. (2000). Study of WO3-Based Sensing Materials for NH3 and NO Detection. *Sensors Actuators B: Chem.* 66, 74–76. doi:10.1016/s0925-4005(99)00410-4

Wisitsoraat, A., Tuantranont, A., Comini, E., Sberveglieri, G., and Wlodarski, W. (2009). Characterization of N-type and P-type Semiconductor Gas Sensors Based on NiOx Doped TiO2 Thin Films. *Thin Solid Films* 517, 2775–2780. doi:10.1016/j.tsf.2008.10.090

Wu, C.-M., Naseem, S., Chou, M.-H., Wang, J.-H., and Jian, Y.-Q. (2019). Recent Advances in Tungsten-Oxide-Based Materials and Their Applications. *Front. Mater.* 6, 49. doi:10.3389/fmats.2019.00049

Wu, C.-M., Shrisha, C.-M., Motora, K. G., Kuo, D.-H., Lai, C.-C., Huang, B.-R., et al. (2021). Cesium Tungsten Bronze Nanostructures and Their Highly Enhanced Hydrogen Gas Sensing Properties at Room Temperature. *Int. J. Hydrogen Energ.* 46, 25752–25762. doi:10.1016/j.ijhydene.2021.05.064

Xiao, S., Liu, B., Zhou, R., Liu, Z., Li, Q., and Wang, T. (2018). Room-temperature H2 Sensing Interfered by CO Based on Interfacial Effects in Palladium-Tungsten Oxide Nanoparticles. *Sensors Actuators B: Chem.* 254, 966–972. doi:10.1016/j.snb.2017.07.169

Yang, X., Wang, W., Xiong, J., Chen, L., and Ma, Y. (2015). ZnO:Cd Nanorods Hydrogen Sensor with Low Operating Temperature. *Int. J. Hydrogen Energ.* 40, 12604–12609. doi:10.1016/j.ijhydene.2015.07.086

Yao, Y., Ao, K., Lv, P., and Wei, Q. (2019). MoS2 Coexisting in 1T and 2H Phases Synthesized by Common Hydrothermal Method for Hydrogen Evolution Reaction. *Nanomaterials* 9, 844. doi:10.3390/nano9060844

Zhang, X., Tang, H., Xue, M., and Li, C. (2014). Facile Synthesis and Characterization of Ultrathin MoS2 Nanosheets. *Mater. Lett.* 130, 83–86. doi:10.1016/j.matlet.2014.05.078

Zhang, W., Zhang, P., Su, Z., and Wei, G. (2015). Synthesis and Sensor Applications of MoS2-Based Nanocomposites. *Nanoscale* 7, 18364–18378. doi:10.1039/c5nr06121k

Zhang, Y., Zeng, W., and Li, Y. (2018). The Hydrothermal Synthesis of 3D Hierarchical Porous MoS2 Microspheres Assembled by Nanosheets with Excellent Gas Sensing Properties. *J. Alloys Compd.* 749, 355–362. doi:10.1016/j.jallcom.2018.03.307

Conflict of Interest: The authors declare that the research was conducted in the absence of any commercial or financial relationships that could be construed as a potential conflict of interest.

Publisher's Note: All claims expressed in this article are solely those of the authors and do not necessarily represent those of their affiliated organizations, or those of the publisher, the editors and the reviewers. Any product that may be evaluated in this article, orclaim that may be made by its manufacturer, is not guaranteed or endorsed by the publisher.